



Contents lists available at ScienceDirect

Nuclear Instruments and Methods in Physics Research A

journal homepage: www.elsevier.com/locate/nima

Highly collimating neutron optical devices

F.M. Piegsa^{a,b,*}^a Paul Scherrer Institute, CH-5232 Villigen PSI, Switzerland^b Physics Department, Technische Univ. München, D-85748 Garching, Germany

ARTICLE INFO

Article history:

Received 23 December 2008

Received in revised form

3 February 2009

Accepted 4 February 2009

Available online 14 February 2009

Keywords:

Neutron physics

Neutron optics

Collimation

Neutron radiography

ABSTRACT

Two Soller type highly collimating neutron optical devices with a length of 200 mm are presented. They provide a triangular shaped beam divergence distribution with a FWHM of about 0.11° (2 mrad) and a peak transmission of up to 80% for neutrons with a wavelength λ_0 of 5 Å. This corresponds to an improvement of more than a factor three compared to state of the art collimators. Measurements are presented which demonstrate the usefulness of these devices also for neutron radiography.

© 2009 Elsevier B.V. All rights reserved.

1. Introduction

The collimation of beams is essential in neutron physics. The degree of divergence is limited by the necessity to have a reasonable residual neutron flux behind the collimation device. Slit diaphragms and Soller type collimators [1,2] are standard tools in neutron scattering to reduce the divergence of the beams and to provide adequate momentum transfer resolution. In neutron radiography one uses a simple pin hole diaphragm to image a several meters away placed object to achieve high spatial resolution [3]. Soller collimators are usually not used in neutron radiography as they can hardly compete with the pin hole geometry in terms of neutron flux and collimation [4].

Here two Soller type collimators are presented, which have been designed for a fundamental neutron physics experiment [5]. The first uses parallel aligned silicon wafers coated with an absorbing layer of TiGd (*silicon collimator*). The second uses thin steel foils also coated with TiGd separated and aligned by means of aluminium frame spacers (*steel collimator*). Both collimators provide very good neutron beam collimation without causing a large decrease in the transmitted intensity, making them of great interest for neutron scattering as well as for neutron radiography.

2. Design of the collimating neutron devices

The silicon collimator consists of an arrangement of silicon wafers with a nominal thickness of 0.38 mm and a rectangular

shape of $200 \times 35 \text{ mm}^2$. The wafers are sputtered on both sides with a $1 \mu\text{m}$ thick absorption layer of TiGd at the DC magnetron sputtering facility at the Paul Scherrer Institute. They are aligned parallel at intervals of 0.8 mm using an aluminium base-plate with eroded slits and three aluminium “combs” (see Fig. 1). The spacing between the wafers causes that half of the passing neutrons travel in the 0.4 mm gaps, while the other penetrate through the 200 mm long wafers. This obviously increases the total neutron transmission compared to standard Soller type collimators using stacks of coated wafers [6–8].

The steel collimator consists of 0.05 mm thick steel foils, which are coated on one side with a $1.5 \mu\text{m}$ thick TiGd layer. The foils are alternately stacked with laser cut 0.4 mm thick aluminium frame spacers. The frames are optimised such that the penetrating neutrons pass through a minimum amount of material. The four ligaments which help to reduce the waviness of the foils have a total thickness in beam direction of only 16 mm. Fig. 2 shows the assembled device and the individual parts.

Both kinds of absorbers, a silicon wafer and a steel foil, have been tested separately at the neutron reflectometer Narziss at the spallation neutron source SINQ at the Paul Scherrer Institute. The monochromator of the reflectometer provides a 5 Å neutron beam with $\Delta\lambda/\lambda_0 = 1.5\%$. The two collimating slits in front of the sample and the slit in front of the detector were set to a height of 20 mm and to a width of 0.5 mm such that a horizontal beam divergence of about 0.01° was achieved.¹ In Fig. 3 the transmission rocking curves of the absorbers are presented, showing that they are almost opaque for incident angles $\omega < 2^\circ$. The transmission of less than 1% ensures that the beam attenuation of the devices is

* Corresponding author at: Paul Scherrer Institute, CH-5232 Villigen PSI, Switzerland. Tel.: +41 56 310 5395; fax: +41 56 310 3718.

E-mail address: florian.piegsa@psi.ch

¹ The distance between the two slits in front of the sample is about 73 cm, while the distance between the first slit and the detector slit is about 2.5 m.

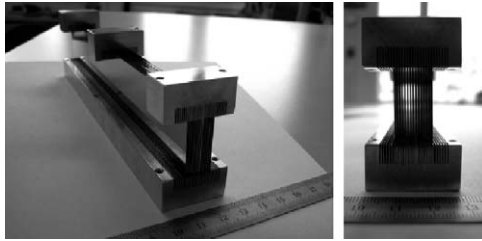


Fig. 1. Pictures of the silicon wafer collimator with a length of 200 mm. The coated wafers are aligned parallel in 0.4 mm wide and 6 mm deep slits, which were eroded in an aluminium plate and three aluminium combs (compare Ref. [9]).

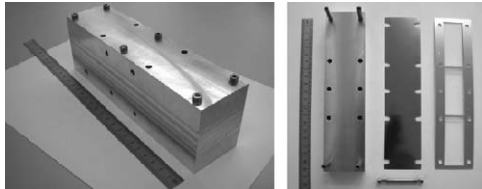


Fig. 2. Left: picture of the assembled steel foil collimator for a beam cross-section of $26 \times 26 \text{ mm}^2$. Right: one of the aluminium base-plates ($200 \times 50 \times 20 \text{ mm}^3$), a coated steel foil and an aluminium frame spacer. The three windows in the spacer have a width of 26 mm.

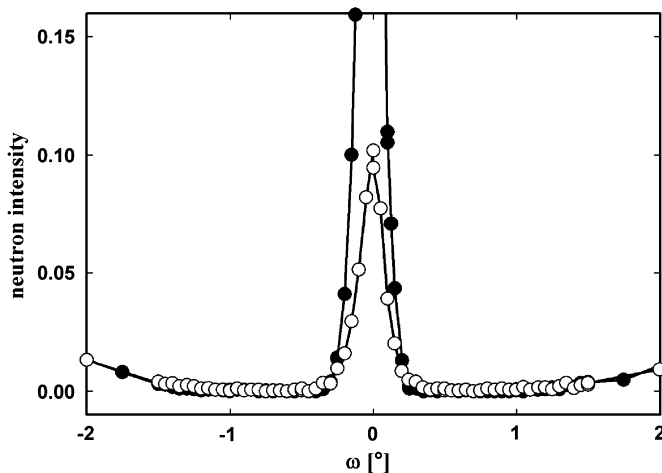


Fig. 3. Normalised transmission of 5 \AA neutrons through a single silicon wafer (filled circles) and a single steel foil (white circles) versus the rocking angle ω . The peaks at $\omega \approx 0^\circ$ are caused by the direct beam, which passes by the absorbers without penetrating the absorption layer.

sufficient for neutron wavelengths of down to 1 \AA , i.e. the whole spectrum of a cold neutron source.

The expected transmission of the two devices can be estimated using the absorption cross-sections of silicon and aluminium given in Ref. [10]. Considering a perfectly parallel 5 \AA neutron beam, this yields to an ideal transmission averaged over the beam cross-section of 81% for the silicon collimator and of 83% for the steel collimator.

3. Performance of the collimation devices

The performance of the devices has been measured also at the Narziss cold neutron reflectometer. The slit diaphragms were set as stated in Section 2. The transmissions of the devices have been determined by performing a scan over the rocking angle ω (see

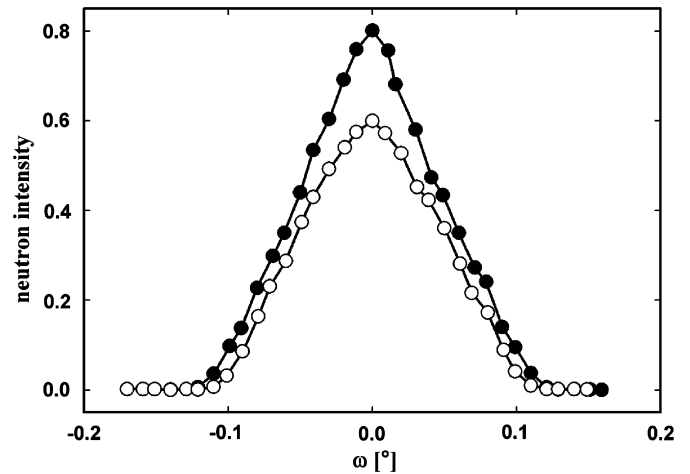


Fig. 4. Transmission rocking curves of the two devices for 5 \AA neutrons in steps of 0.01° : the silicon collimator (filled circles) and the steel collimator (white circles).

Table 1

Data here presented silicon collimator compared to results published by other groups.

$\Delta\omega$ ($^\circ$)	T_p (%)	λ_0 (\AA)	Ref.
0.23	65	4.7	[6]
0.41	78	4.7	[6]
0.90	84	4.7	[6]
0.37	83.5	4.7	[7]
0.36	88	1.8/7.5	[8]
0.11	80	5.0	This work

$\Delta\omega$ is the FWHM of the triangular shaped divergence distribution with the peak transmission T_p using neutrons with the wavelength λ_0 .

Fig. 4). The plots show a triangular shaped acceptance distribution with a width of $\Delta\omega = 0.11^\circ$ (FWHM), which is close to the expected value of $\arctan(0.4 \text{ mm}/200 \text{ mm}) = 0.115^\circ$. The peak transmissions of $(80 \pm 2)\%$ for the silicon collimator and $(60 \pm 2)\%$ for the steel collimator are normalised to the direct beam and give the average value over the whole cross-sections of the devices, obtained by a lateral scan at $\omega = 0^\circ$. They have also been corrected taking the non-perfect collimation of the incoming neutron beam into account.²

A comparison between the experimentally found peak transmissions and the expected values given in the previous section shows that the mechanical setup of the silicon collimator works very well, whereas the steel collimator cannot meet the expectations. This is probably due to the waviness of the steel foils, which could be further reduced by introducing more thin ligaments in the aluminium frames. Another drawback of the steel collimator is that the foils are magnetic and, therefore, can cause depolarisation of a polarised neutron beam.

Table 1 compares the performance of the silicon collimator with state of the art neutron collimators made from stacks of silicon wafers. It shows that for almost equal peak transmissions of approximately 80% the width of the divergence distribution could be decreased by more than a factor of three. The achieved high peak transmission is even more remarkable, when considering that the presented device is 2–5 times longer compared to the collimators in the references.

² The correction of the peak values is on a level of about 3.5% and is obtained by performing a convolution of two triangular functions of different widths.

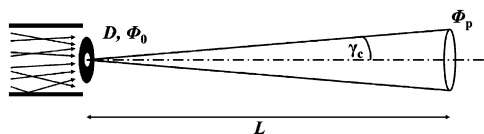


Fig. 5. Scheme of the pin hole geometry commonly used in neutron radiography. Neutrons are transported by a neutron guide from the neutron source to the beam aperture with diameter D . All neutrons with an angle of incidence smaller than the critical angle γ_c get totally reflected on the walls of the neutron guide. The neutron flux at the aperture is Φ_0 . At a distance L the neutron flux is reduced to Φ_p , due to the conical shape of the beam.

4. Neutron radiography

4.1. Neutron flux

These highly collimating optical devices can be utilised in neutron radiography instead of the standard pin hole geometry. To compare the obtainable neutron fluxes between these two methods we first consider the pin hole setup given in Fig. 5. Here the collimation is achieved by placing the investigated object in a distance L (usually a few meters) from a circular diaphragm with a diameter D (typical several millimeters to centimeters). The neutron flux³ Φ_p at the object position can be estimated by

$$\Phi_p = \Phi_0 \left(\frac{D}{L}\right)^2 \frac{1}{4 \tan^2 \gamma_c} \quad (1)$$

where Φ_0 is the neutron flux at the aperture.

Using two identical collimators (vertical and horizontal) will reduce the aperture–object distance, L , drastically. Hence, there is no decrease of neutron flux due to the conical beam. On the other hand, the beam spot is limited to the size of the aperture and there are flux losses caused by the non-perfect transmission of the collimators. This yields an approximate neutron flux behind the two collimators of

$$\Phi_c = \Phi_0 \left(\frac{\Delta\omega \cdot T_p}{2\gamma_c}\right)^2 \quad (2)$$

Comparing Eqs. (1) and (2) leads to

$$\frac{\Phi_c}{\Phi_p} \approx \Delta\omega^2 \cdot T_p^2 \left(\frac{L}{D}\right)^2 \quad (3)$$

using $\tan \gamma_c \approx \gamma_c$ and $[\Delta\omega] = \text{rad}$.

Eq. (3) contains two different quantities describing the divergence of a neutron beam. To be able to entirely compare the fluxes of both methods, the L/D -ratio [4] used for the pin hole geometry has to be linked to $\Delta\omega$ used for neutron collimators. Therefore, we consider the consequence of the beam divergence on the image quality and introduce a geometric unsharpness u , which is a linear function of the object–detector distance d . It should be pointed out that there is no single definition for u . We adopt the one given in Ref. [12], which defines u as the length on the detector in which the neutron intensity increases from 10% to 90%, when a sharp knife-edge object is imaged. The intensity profile perpendicular to a sharp edge is called *edge spread function* (ESF). In Fig. 6 the theoretical ESF's of a triangular and a rectangular shaped beam divergence distribution are plotted. The rectangular distribution corresponds to the pin hole geometry, where the achievable geometric unsharpness u_{\square} is determined by the L/D -ratio and not by the critical angle⁴ γ_c .

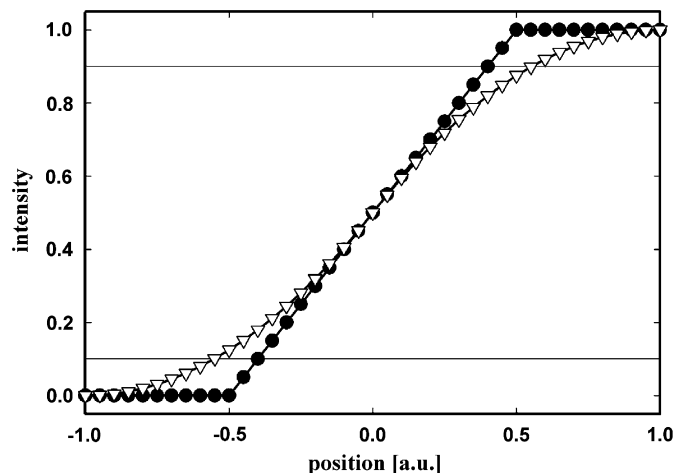


Fig. 6. Edge spread functions of a rectangular beam divergence distribution (filled circles) and a triangular shaped distribution (white triangles). The initial distributions have the same width (FWHM). The horizontal lines mark 10% and 90%.

We find

$$u_{\square} = 0.8 \cdot \frac{d}{(L/D)} \quad (4)$$

$$u_{\Delta} \approx 1.1 \cdot d \tan(\Delta\omega). \quad (5)$$

By setting $u_{\square} = u_{\Delta}$, one can define an effective L/D -ratio for a triangular divergence distribution

$$\left(\frac{L}{D}\right)_{\text{eff}} \approx \frac{0.7}{\tan(\Delta\omega)}. \quad (6)$$

For $\Delta\omega = 0.11^\circ$ it yields $(L/D)_{\text{eff}} \approx 360$. Inserting this in Eq. (3), it follows with $T_p = 80\%$ that $\Phi_c/\Phi_p \approx 0.33$.

Hence, in this case, the pin hole geometry delivers approximately three times more neutrons than the collimator method. But to reach a L/D -ratio of 360 with a circular diaphragm with a diameter of e.g. 25 mm, one has to provide an aperture–object distance of $L \approx 9$ m. However, when using two collimators a total setup-length of less than 1 m is already sufficient.

4.2. Examples

To demonstrate the feasibility of neutron radiography with the above presented collimators a test was setup at the cold neutron beam line FUNSPIN [13] at the spallation neutron source SINQ at the Paul Scherrer Institute. The two collimators with a total length of approximately 40 cm are placed right after each other in a crossed geometry (first the silicon collimator reducing the horizontal beam divergence and then the steel collimator reducing the vertical beam divergence). They are providing a well collimated beam in both directions with a cross-section of about $10 \times 20 \text{ mm}^2$. A neutron CCD-camera with a pixel-size of $0.13 \times 0.13 \text{ mm}^2$ [14] is situated at a 40 cm distance behind the second collimator. An open beam image together with plots of horizontal and vertical cuts are presented in Fig. 7. Both plots show plateau regions, which decline fast toward the sides of the beam spot. The vertical cut along the y -axis exhibits deviations from a perfect flat plateau due to the internal structure of the steel collimator, which is situated closer to the camera.

However, these intensity deviations do not harm the radiography images as one can see in Fig. 8. There, three example radiographies are presented, showing the images of a neutron radiography test device [15], a stainless steel screw and a cryostat needle valve.

³ Neutron flux: $[\Phi] = \text{neutrons cm}^{-2} \text{ s}^{-1}$.

⁴ The critical angle is given by: $\gamma_c \approx m \times 0.1^\circ \times \lambda_0(\text{\AA})$, where m denotes the ratio of the critical momentum transfer of the neutron guide coating and natural nickel [11].

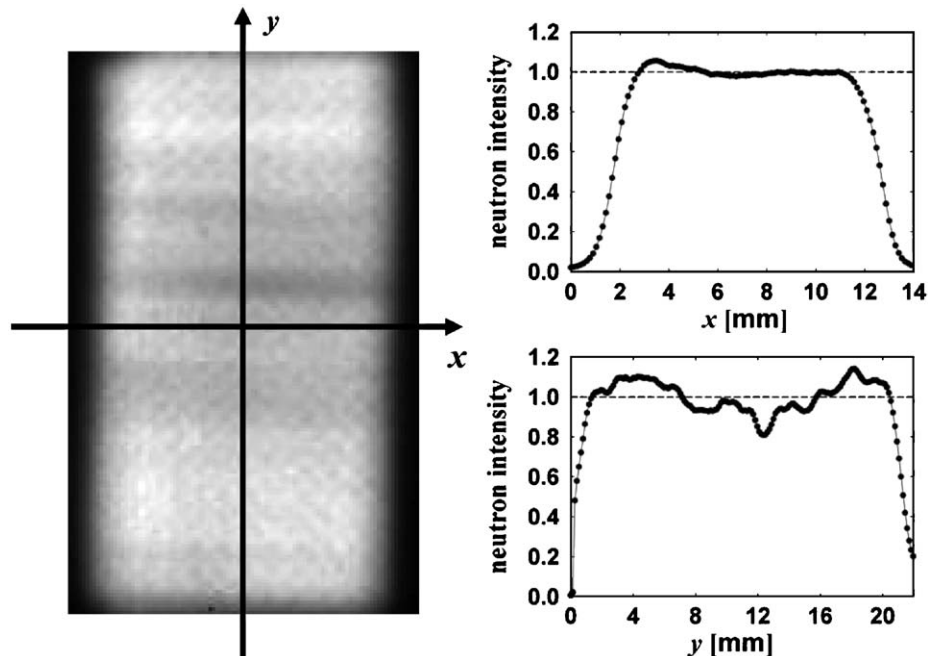


Fig. 7. Left: open beam image with a size of $13 \times 21 \text{ mm}^2$. The neutron camera was placed 40 cm behind the exit of the second collimator. Right: plots of horizontal and vertical cuts of the open beam image. The intensities are normalised to the average beam intensity over the entire beam spot.

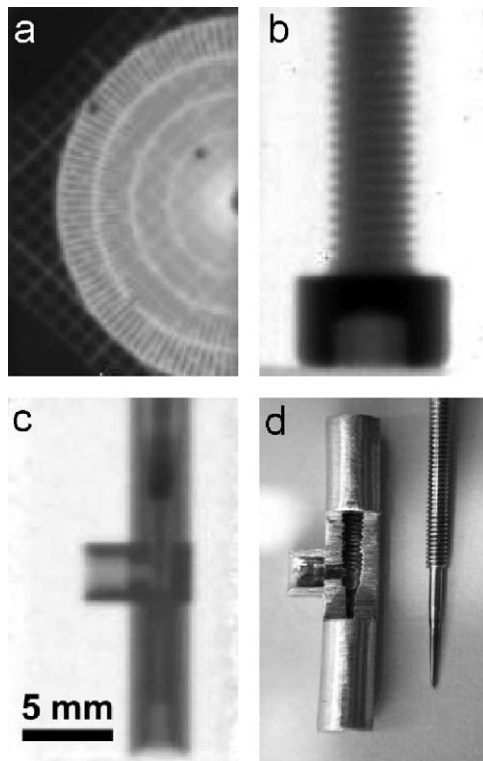


Fig. 8. Three test radiographies taken with the two crossed collimators. The radiography images have a size of $13 \times 21 \text{ mm}^2$, which corresponds to 100×160 pixels. The sample–detector distance was about 3 cm. (a) A gadolinium test device. The outermost ring of the Siemens star has a period of $500 \mu\text{m}$. (b) Stainless steel M5-hexagon socket screw. (c) Cryostat needle valve for liquid helium [16]. (d) Photograph of a cut-open version of the needle valve made out of brass (socket) and stainless steel (needle).

5. Conclusions

Two Soller type collimators for cold neutron beams have been realised. They provide a triangular shaped neutron beam with a width of about 0.11° (FWHM) and a high peak transmission. They were successfully applied in a neutron radiography setup with a total length of only 80 cm. Their design allows to increase their cross-section easily up to $30 \times 30 \text{ mm}^2$, which is a sufficient size for e.g. micro-tomography setups [17]. The silicon collimator could be even further improved by using slightly thinner wafers with a thickness of 0.3 mm and a length of 200 mm [9]. At a similar peak transmission, this should provide beam collimations down to 0.08° , which corresponds to an effective L/D -ratio of approximately 500.

Acknowledgements

These experiments were supported by the Sample Environment and Polarised Targets group of the Paul Scherrer Institute. The technical support by P. Schurter, whose outstanding skills have made this work possible, is gratefully acknowledged.

References

- [1] W. Soller, Phys. Rev. 24 (1924) 158.
- [2] C.J. Carlile, P.D. Hey, B. Mack, J. Phys. E 10 (1977) 543.
- [3] J.P. Barton, et al. (Eds.), Neutron Radiography, in: Proceedings of the First World Conference, D. Reidel Publishing Company, Dordrecht, Holland, 1982, ISBN 90-277-1528-9.
- [4] J.C. Domanus (Ed.), Practical Neutron Radiography, 1992, ISBN 07-923-1860-9, (Chapter 10).
- [5] F.M. Piegsa, B. van den Brandt, H. Glättli, P. Hautle, J. Kohlbrecher, J.A. Konter, B.S. Schlimme, O. Zimmer, Nucl. Instr. and Meth. A 589 (2008) 318.
- [6] Th. Krist, F. Mezei, Physica B 276–278 (2000) 208.
- [7] Th. Krist, J. Peters, H.M. Shimizu, J. Suzuki, T. Oku, Physica B 356 (2005) 197.

- [8] L.D. Cussen, C.J. Vale, I.S. Anderson, P. Hoghoj, Nucl. Instr. and Meth. A 471 (2001) 392.
- [9] F.M. Piegsa, M. Schneider, Nucl. Instr. and Meth. A 594 (2008) 74.
- [10] V.F. Sears, Neutron News 3 (1992) 26.
- [11] H. Maier-Leibnitz, T. Springer, J. Nucl. Energy A/B 17 (1963) 217.
- [12] A.A. Harms, A. Zeilinger, Phys. Med. Biol. 22 (1977) 70.
- [13] J. Zejma, et al., Nucl. Instr. and Meth. A 539 (2005) 622.
- [14] M.J. Mühlbauer, E. Calzada, B. Schillinger, Nucl. Instr. and Meth. A 542 (2005) 324.
- [15] C. Grünzweig, G. Frei, E.H. Lehmann, G. Kühne, C. David, Rev. Sci. Instrum. 78 (2007) 053708.
- [16] B. van den Brandt, J.A. Konter, S. Mango, Nucl. Instr. and Meth. A 289 (1990) 526.
- [17] E.H. Lehmann, G. Frei, G. Kühne, P. Boillat, Nucl. Instr. and Meth. A 576 (2007) 389.